Scientific Research Publishing

Optics and Photonics Journal, 2018, 8, 146-164
http://www.scirp.org/journal/opj
ISSN Online: 2160-889X
ISSN Print: 2160-8881

Photoluminescence and Structural Analysis of Samarium Doped TiO_2 Thin Films and Their Applications to Visible LEDs

M. Murayama[1], K. Yoda[1], K. Shiraishi[1], S. Guan[1], S. Komuro[2], X. Zhao[1]

[1]Department of Physics, Tokyo University of Science, Tokyo, Japan
[2]Faculty of Science and Engineering, Toyo University, Saitama, Japan
Email: xwzhao@rs.kagu.tus.ac.jp

How to cite this paper: Murayama, M., Yoda, K., Shiraishi1, K., Guan, S., Komuro, S. and Zhao, X. (2018) Photoluminescence and Structural Analysis of Samarium Doped TiO_2 Thin Films and Their Applications to Visible LEDs. *Optics and Photonics Journal*, **8**, 146-164.
https://doi.org/10.4236/opj.2018.85014

Received: April 11, 2018
Accepted: May 28, 2018
Published: May 31, 2018

Abstract

Samarium-doped anatase TiO_2 (A-TiO_2:Sm) and rutile (R-TiO_2:Sm) single phase thin films are fabricated by laser ablation and post-annealing at different temperatures. A-TiO_2:Sm samples exhibit intense PL emission, whilst R-TiO_2:Sm samples exhibit weak PL emission. The local crystal structure of Sm-dopants is investigated using X-ray absorption fine structure (XAFS) measurements. The thin films showing strong PL emission have lower crystal symmetry than the other samples, which show weak PL emission. We report the relationship between changing the symmetry of the local structure and activation of the luminescent center. The local structure of Sm^{3+} thin films annealed at 600˚C to 800˚C, which possess an activated semi-stable Sm^{3+} ions luminescent center, dramatically changes from having high symmetry to low symmetry. While the phase transitioned R-TiO_2:Sm and fabricated as R-TiO_2:Sm samples showed highly symmetric. Hence, the coordination around the doped-Sm^{3+} ions is the key factor for exhibiting an intense PL emission. Therefore, activation of the luminescent center is strongly connected with the distorted local crystal symmetry, which is proposed as one of the factors defining the transfer probability. In this work, we discuss the connection between coordination around Sm^{3+} ions and PL intensity, and optical and electrical properties of a n^+-ITO/TiO_2:Sm/p-NiO/p^+-Si hetero junction LED preparing with optimal fabricating condition.

Keywords

Rare-Earth, Semiconductor, Photoluminescence, XAFS, LEDs

1. Introduction

Rare earth element doped semiconductors and oxide materials have been studied

for a long time as they have the potential for application in visible and infrared light emitting diodes and other optical devices [1]-[6]. Particularly, the combination of erbium (Er) and silicon (Si) is extensively studied because the Er-related 1.54 μm emission corresponds to a minimum loss window of the optical fibre, which makes it industrially profitable [7] [8] [9] [10]. The local structure of doped-Er^{3+} ions in oxide semiconductors is of particular interest. Er^{3+} is surrounded by oxygen (O) ligands, and the intensity of its luminescence is influenced by the symmetry of the surrounding O ligands [9] [10]. The chemical properties of both the doped rare earth and host materials can be considered to determine the atomic coordination of the doped rare earth element-O luminescent center. This fact indicates that analyzing the symmetry of rare earth-O would enable determination of the optimal conditions for the production of applicable materials with a luminescent center.

Selecting host semiconductors with a wide band gap is also known to be essential for effective excitation of the rare earth element. It was noted that certain semiconductors, including ZnO, GaN and TiO_2, would be good candidates as host materials for optical devices [1] [2] [3] [4] [11] [12] [13] [14]. Such semiconductors will enhance the rare earth ions-related emission as they possess a wide band gap [15] [16]. TiO_2 is attracting increasing attention as a host wide-gap semiconductor. It is an environmentally-friendly material, so can not only be used as a host for luminescence and applied to LEDs and other optoelectronic devices, but can also be applied to solar cells, photocatalysts and other energy-related products [17] [18] [19]. TiO_2 has three crystal phases: anatase (A-TiO_2, tetragonal, band gap: 3.2 eV), rutile (R-TiO_2, tetragonal, band gap: 3.0 eV) and brookite (orthorhombic) [19] [20]. Most of the applications select the crystal phase of A- or R-TiO_2 with suitable properties depending on the usage.

Sm^{3+} was chosen as the dopant in the semiconductor. Its optical and luminescent properties of Sm have been studied by using several techniques for preparations of samples, such as the atomic layer deposition, sol-gel method, doping on borate glasses, and laser ablation technique [21]-[26]. Each of the techniques has unique advantages. In this work, the samples were fabricated by using laser ablation, because the crystalline phase of the host material, TiO_2 need to be appropriately selected. Additionally, the local structure has been investigated [25] [26]. Addition of SmO_6 resulted in distortion of the host semiconductors of TiO_2 with C_{4v} symmetry and exhibited the most intense photoluminescence (PL) emission [26]. From the application as optical devices, these different crystalline structures may affect the rare earth-related PL emission; Sm^{3+} exhibits a sharp 1.2 μm emission, as it closely resembles Er. Based on these facts, we report the comparison of the local structures, especially estimation of symmetry by using XAFS measurement, and PL intensity of Sm-doped A- and R-TiO_2 with different annealing temperatures, and the coordination around Sm^{3+}, while the Sm^{3+} ions luminescent center is activated. Also LED device has been fabricated based on the same sample of above. Electrical and optical properties are reported.

2. Experimental Procedure

The Sm-doped TiO_2 (TiO_2:Sm) thin films were deposited by laser ablation using a Q-switched yttrium aluminum garnet (YAG) laser ($4\omega_0$ = 266 nm, 1 J/cm^2). A TiO_2 ceramic target, including 1.0 wt% Sm_2O_3, was used as the deposition source. Laser ablation is a typical method for synthesizing a thin film with the same composition ratio as the target. The A-TiO_2 and R-TiO_2 thin films were deposited in a vacuum chamber with different atmospheres; A-TiO_2 with an O_2 pressure of 1×10^{-2} Torr and R-TiO_2 without O_2 under a pressure of 1×10^{-7} Torr. As has been reported in our previous work, selecting an appropriate atmosphere enables the production of the suitable crystalline phase (A- or R-) of TiO_2 [24].

By ablation of the amorphous phase, TiO_2:Sm thin films of 300 nm thick were formed on Si (100) surfaces at room temperature. After the deposition, the samples were annealed at a temperature between 300˚C to 1100˚C, with temperature intervals of 100˚C, for 2 min or 30 min in the O_2 atmosphere for optical activation of Sm^{3+} ions and formation of the nanometer-sized TiO_2 crystals. The crystal phase and grain sizes were estimated by X-ray diffraction (XRD). A He-Cd laser (λ = 325 nm) was used to excite the Sm^{3+} and to measure the PL spectra from the TiO_2:Sm thin films.

The X-ray absorption fine structure (XAFS) measurements using synchrotron radiation (SR) were performed at the High Energy Accelerator Research Organization on BL 27B Photon Factory in Tsukuba prefecture, Japan. A Si double crystal set was used to monochromatize the SR beam. A seven-element pure-Ge solid-state detector was used for counting the fluorescence X-rays proportional to the X-ray absorption of the TiO_2:Sm thin films. The X-ray incidence angle was fixed at 45˚. The Athena and Artemis of Demeter, which are free programs for XAFS analysis created by Ravel B, were used for an ordinary process of XAFS analysis, that is, extracting the oscillations and fitting the Fourier spectra.

3. Result

3.1. Estimation of Crystal Phase and PL Properties of Sm-Doped Anatase and/or Rutile TiO_2

Figure 1 shows the XRD patterns of Sm-doped TiO_2 thin films annealed at different temperatures. The conditions for fabricating the samples were fixed for the experiments of A-TiO_2:Sm to keep the same preparation conditions. The atmosphere for the film deposition and an annealing time of 30 min for R-TiO_2:Sm are the only differences from the fabricating conditions for A-TiO_2:Sm. Selecting the appropriate atmosphere for ablation can enable the production of the suitable crystal phase (A- or R-) TiO_2:Sm, which we reported in a previous study [24]. The as-deposited thin film is yet to be used in any post-annealing processes. The strongest peak of A (101) at $2\theta = 25.3^\circ$ can be observed for the sample fabricated as anatase and post-annealed at 700˚C in Figure 1(a). The crystal phase was indexed by the JCPDS card No. 21-1272 (25.323,

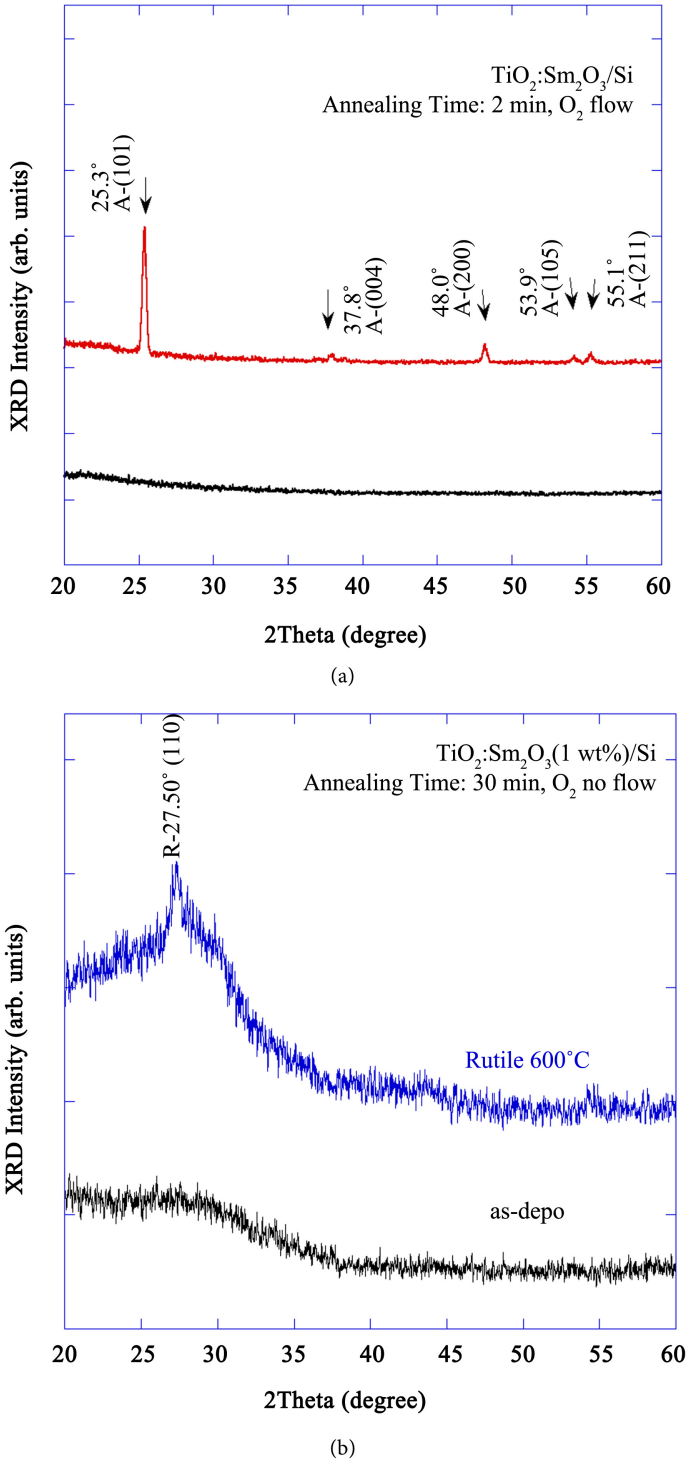

Figure 1. XRD patterns of Sm-doped (a) A-TiO_2 and (b) R-TiO_2 thin films annealed at different temperatures.

37.839, 48.071, 53.948), and its grain size was 25.8 nm. The as-deposited TiO_2:Sm thin films were in the amorphous phase. The series of samples which were fabricated as A-TiO_2:Sm and post-annealed at temperatures from 700˚C to 1000˚C showed the anatase phase, as was expected. A-TiO_2:Sm was changed to

R-TiO_2:Sm with an annealing temperature of 1100˚C. Details have been reported in our previous work [25]. Additionally, **Figure 1(b)** shows that the peak at 2θ = 27.5˚ can be identified as rutile phase based on the JCPDS card No. 21-1276 (27.446). The sample was fabricated as R-TiO_2:Sm, as was expected. And its grain size was 1.5 nm which was very smaller than the sample fabricated as anatase crystalline phase.

Figure 2(a) shows the comparison of the PL spectra between A- and R-TiO_2:Sm thin films annealed at 600˚C. The annealing time of each sample was

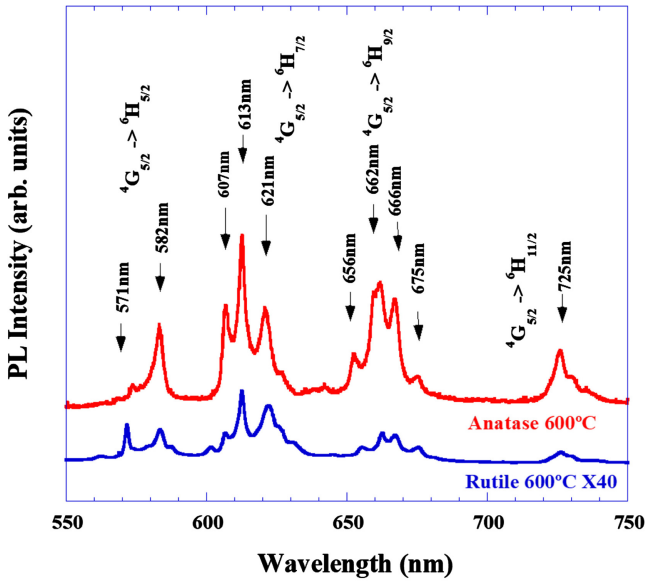

(a)

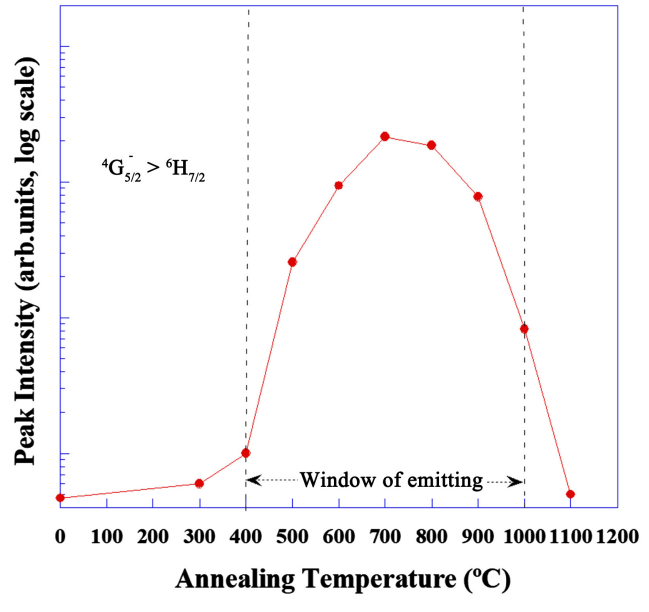

(b)

Figure 2. (a) shows PL spectra of A- and R-TiO_2:Sm thin films at room temperature; (b) is the PL intensity ratio at 613 nm of A-TiO_2:Sm annealed at different temperatures.

2 min for A-TiO_2 and 30 min for R-TiO_2. The PL intensity of the R-TiO_2:Sm is 40 timed the actual intensity. The PL emissions corresponding to $^4G_{5/2} \rightarrow {}^6H_J$ (J = 5/2, 7/2, 9/2 and 11/2) intra-4f transitions in Sm^{3+} ions can be observed. The different PL intensities indicate the difference of the transition probability, and the different fine structure of the PL spectra suggests the difference of coordination around the Sm^{3+} ions, which is the luminescent center. Additionally, this result indicates that R-TiO_2:Sm is not suitable for application to optical devices compared with A-TiO_2:Sm, even if it is prepared under the optimal conditions for activation of the luminescent center. In our previous work, the crystal symmetry of Sm^{3+} ions has been shown to be strongly connected with the luminescent center and the efficiency of luminescence [25]. These facts indicate that there must be a difference of the local structure between samples that show strong PL spectra and weak PL spectra. **Figure 2(b)** shows the PL emission intensity ratio at 613 nm of A-TiO_2:Sm annealed at different temperatures. PL intensity becomes stronger with an increasing annealing temperature. Jing et al reported that PL from Sm^{3+} was activated from 400˚C [24]. With a further increase of the temperature, the PL intensity became weaker after reaching 700˚C. This result suggests that Sm^{3+} with a crystal field allowing intra-4f transitions is formed in the crystal matrix by the annealing. Hence, the fabricated samples annealed at an appropriate temperature results in a window for making the luminescence center. As reported in our previous work, at an annealing temperature of 1100˚C, anatase phase A-TiO_2:Sm transitioned to rutile phase R-TiO_2:Sm. Both the phase transitioned R-TiO_2:Sm and deposited R-TiO_2:Sm exhibited weak PL spectra.

3.2. Investigation of the Details of Electronic Levels by XAFS Experiment and Preparations for EXAFS Analysis

Figure 3 shows the XAFS spectra at the Sm L_{III}-edge (6720 eV) of A-TiO_2 obtained at temperatures between 400˚C to 1100˚C as well as the as-deposited sample. The series of samples are the same as that in **Figure 1(a)**. The spectra of R-TiO_2:Sm obtained at annealing temperatures of 650˚C and 400˚C and the as-deposited sample are shown in **Figure 4**. The lowest spectrum is that from the Sm_2O_3 powder of the standard sample. An analysis of the X-ray absorption near edge structure (XANES) provides information on the electronic property. The most intense peak, called the "white-line", is intrinsic to the Sm oxides: SmO_x (generally $x > 6$). The drawn dotted line at the white-line shows the excitation energy of Sm^{3+}. The peak absorption of every spectrum appeared at the same peak from the Sm_2O_3 powder, which suggests that the Sm^{3+} state was mainly formed in SmO_x without any out diffusions. The full width at half maximum (FWHM) of the white-line for A-TiO_2 can be estimated as (b) 7.2 eV, (c) 9.5 eV, (d) 9.3 eV, (e) 10.4 eV, (f) 9.0 eV, (g) 9.0 eV and (h) 6.6 eV. The FWHM of the Sm_2O_3 powder has not been estimated because the XAFS spectra are incomparable owing to the difference in purity of the standard sample and our impurity samples; the absorption element, Sm was only doped at 1 wt%: $7.38 \times 10^{19}/cm^3$.

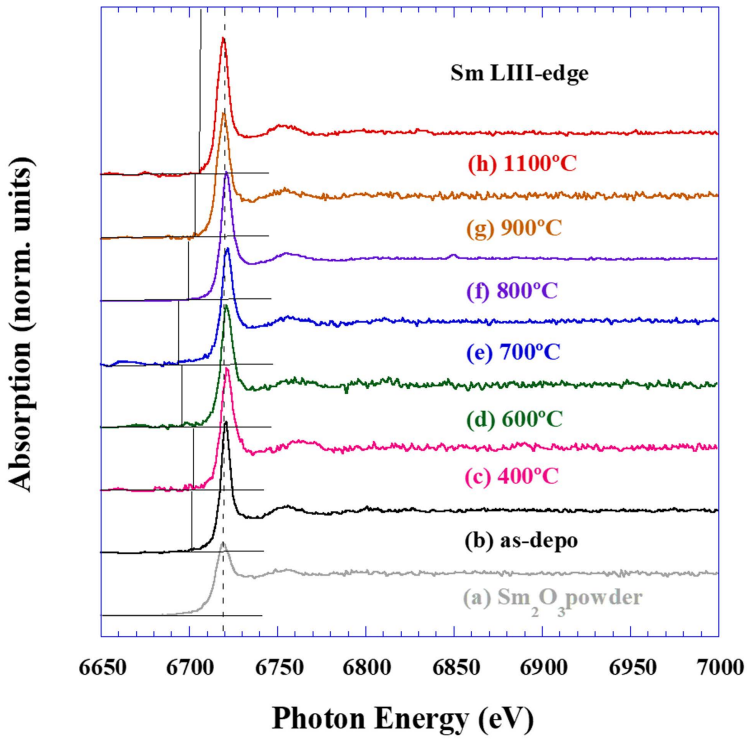

Figure 3. XAFS spectra at the Sm L_{III}-edge of A-TiO_2:Sm thin films obtained at different annealing temperatures. The lowest spectrum is that from the Sm_2O_3 powder of the standard sample.

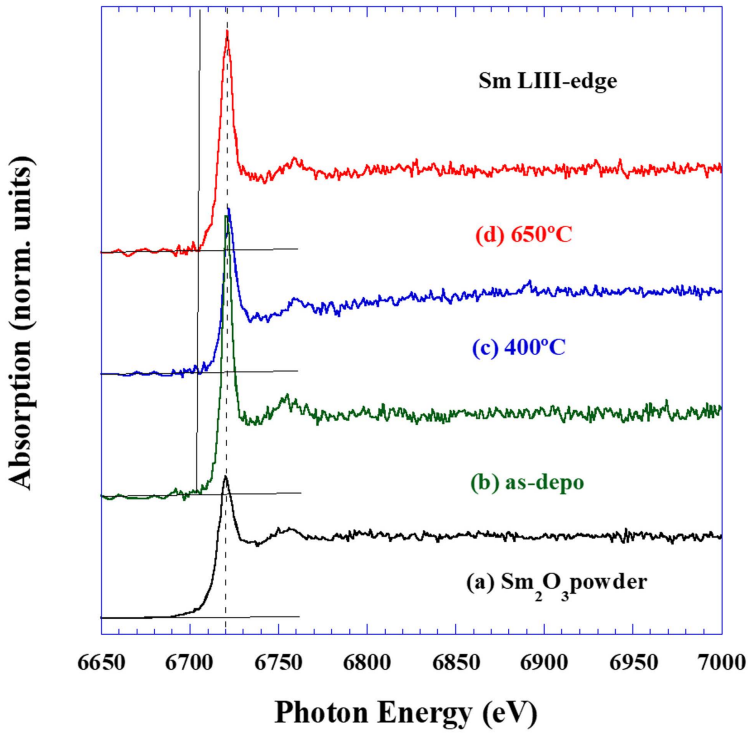

Figure 4. XAFS spectra at the Sm L_{III}-edge of R-TiO_2:Sm thin films obtained at different annealing temperatures. The lowest spectrum is that from the Sm_2O_3 powder of the standard sample.

The wider FWHM of (c) to (g) in **Figure 3** indicates a broadening of the 5*d* density of states (DOS) in A-TiO_2:Sm because of the excitation from an Sm 2*p* inner shell to 5*d* unoccupied states. However, for the sample that phase transitioned to R-TiO_2:Sm, the as-deposited sample, and the samples in **Figure 4**, R-TiO_2:Sm is sharper than the other A-TiO_2:Sm samples, which suggests condensed Sm 5*d* DOS. Additionally, there are tails on the lower energy side of the white-lines of spectra (c) to (g) in **Figure 3**, suggesting a lower ion charge number, Sm^{Z+} (Z < 3) [9] [27]. However, this lower oxidation number can be considered to not be too low so as to affect the luminescence. **Figure 2** has already showed that the thin films annealed at 700˚C, which is curve (e) in **Figure 3**, exhibit the most intense photoluminescence in this study. These characteristics result from the existence of various bond lengths of Sm-O in A-TiO_2; Ishii et al reported that various orbital hybridizations of rare earth elements with O broaden the rare earth 5*d* DOS and partially yield its ion charges [9]. Curves of (b) and (h) in **Figure 3** and **Figure 4** suggest that these samples can be considered to have the same bonding lengths, more stability and higher symmetry than A-TiO_2:Sm.

Figure 5 shows the k^2-weighted extended X-ray absorption fine structure (EXAFS), that is, the χ(k) oscillations of Sm in TiO_2:Sm. The photoelectron vector, k, is defined as $k = (8\pi 2m(E - E_0)/h^2)^{1/2}$, where m is the electron mass, E is the photon energy, E_0 is the energy threshold of the absorption edge and h is the Planck constant. A greater weighting k^n results in emphasizing the higher oscillations. The equation for EXAFS oscillation is:

$$\chi(k) = S_0^2 \sum_j \frac{N_j}{R_j^2 k} F_j(k) \exp\left(-2\sigma_j^2 k^2 - \frac{2R_j}{\lambda_j(k)}\right) \sin\left(2kR_j + \phi(k)\right) \quad (1)$$

Thus, EXAFS oscillation is a sum of exponentially damped sine waves. S_0^2 is a loss term which accounts for multi-electron excitations and inelastic scattering, N_j is the number of atoms in each shell, R_j is the distance between absorbing and scattering atoms, F_j(k) is the magnitude of the complex function describing the scattering, σ_j is a Debye-Waller factor between the absorber and a scattering atom, λ_j is the mean free path of the electron, φ(k) is the phase shift and the index j references a shell of the element. N_j and R_j are already known if it is a standard sample, F_j(k) and φ(k) can be obtained by calculation using the FEFF program [28] [29]. The reliability of XAFS analysis is one of the big issues for all studies which use XAFS measurement. Binsted et al reported EXAFS data analysis with curved wave theory [30]. This equation and parameters will be used for the fitting of the samples. The EXAFS oscillations are obtained from the background removed XAFS spectra with proper k^n weighting (n = 1, 2, 3). We chose k^2 because the higher range of oscillations (after 8.0 $Å^{-1}$) were noisy. The window function was performed in the range of 2.0 - 8.0 $Å^{-1}$, dk = 0.5. The chosen ranges in the XAFS analysis used in this study are all the same to facilitate comparison. There are no significant differences of the different annealing temperatures or the different crystal phases. More detailed estimations of the local

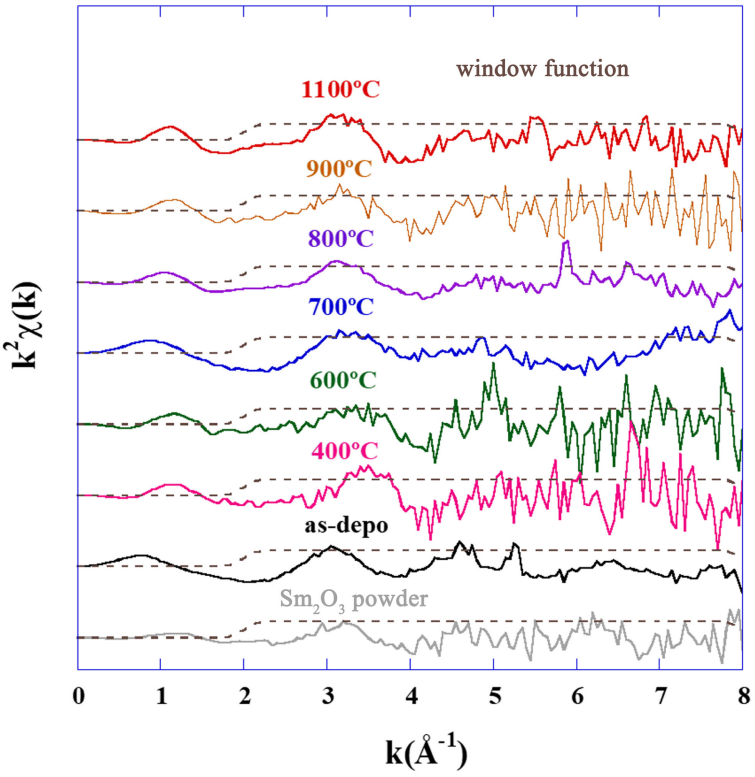

(a)

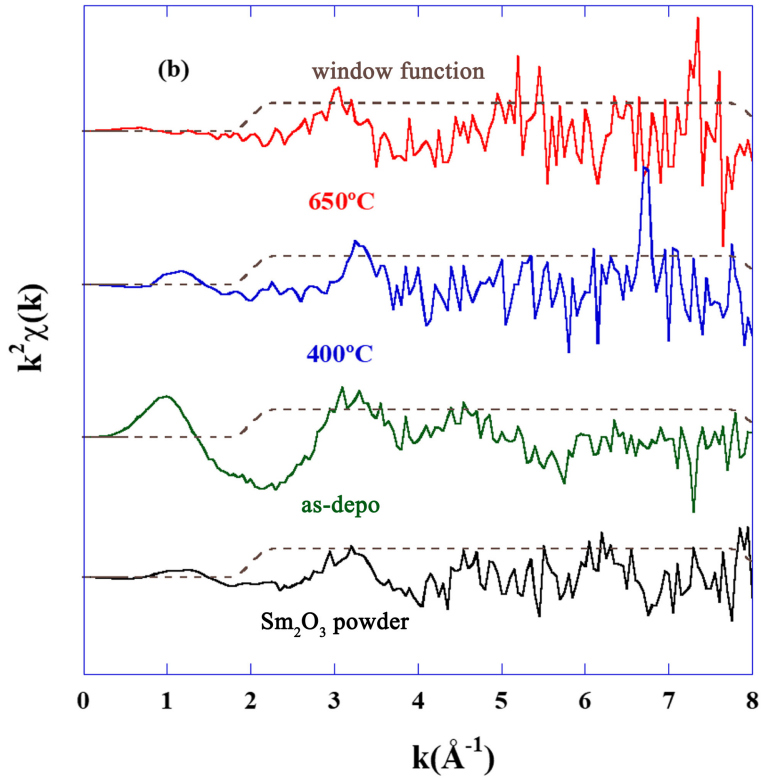

(b)

Figure 5. k^2-weighted EXAFS oscillations (solid line) and window functions (dashed line) of A-TiO_2:Sm (a) and R-TiO_2:Sm (b) thin films.

structure are expected from the Fourier transformed spectra.

The EXAFS analysis was performed to clarify the details of the local structure of the absorption element, such as the atomic distance of the nearest-neighbors to the Sm. Figure 6 shows the radial structural function (RSF) around Sm obtained by the Fourier transform (FT) of k^2-weighted XAFS spectra and the $k^2\chi$ of (a) A- and (b) R-TiO_2:Sm. The first nearest-neighbor (NN) atom from Sm was observed at approximately 1.5 - 2.0 Å for all samples in Figure 6(a). This value is

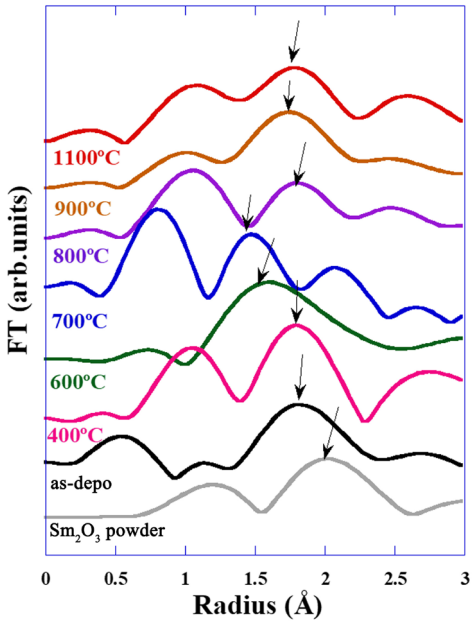

(a)

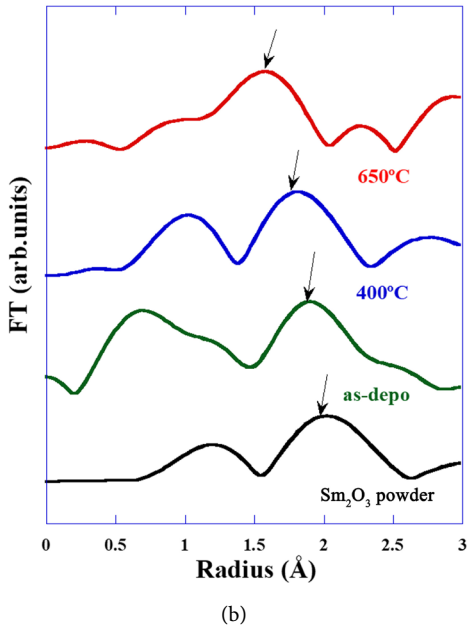

(b)

Figure 6. RSF around Sm delivered from FT of EXAFS oscillation, $k^2\chi$, of (a) A- and (b) R-TiO_2:Sm samples shown in Figures 3-5.

shorter than the actual distance, because the result does not account for the phase shift of the photoelectrons by scattering of atoms in the FT. The actual distance can be obtained by the fitting result that will be discussed later. There were peaks located at an average distance of less than 1.1 Å owing to the low frequency waves in the background. This range was not taken into consideration owing to this reason. As shown in **Figure 6**, these small radii can be considered when the first NN atoms from Sm is O. The samples which exhibit the most far distance are the as-deposited and 1100˚C samples, and exhibit a shorter distance with an increasing annealing temperature, as shown in **Figure 6(a)**. The sample annealed at 700˚C has the shortest distance, and the samples annealed at higher temperature than 700˚C exhibit a longer distance. The peak of the as-deposited and 1100˚C samples appeared near the peak of the Sm_2O_3 powder, suggesting the distance of these samples is closer to the Sm-O bond length in Sm_2O_3 rather than the Ti-O bond length in TiO_2. The ion radii of Ti^{4+} is smaller than that of Sm^{3+}, so the Ti-O bond length is shorter than the Sm-O bond length in Sm_2O_3, from the FEFF calculation. Hence, we can predict that the bond length of the other samples is closer to the Ti-O bond length rather than that of Sm-O. These tendencies are also observed in other properties. The RSF of R-TiO_2:Sm shows a similar tendency as that of A-TiO_2:Sm. The samples annealed at higher temperature exhibit a shorter bond length. The back FT was performed in the range of 2.0 - 2.9, with $dr = 1.0$ for the fitting process.

3.3. Analysis and Mechanism of the Activation of the Luminescent Center

We used the model of crystallographically valid TiO_2:Sm or Nd, and calculated the path of TiO_2 which replaced Ti with doped rare earth element in our previous work [25] [31] because we already know the first NN of Sm is O, and doped Sm replaces at the Ti site; that is, a rare earth-O complex forms at the lattice site of II-IV semiconductors, as was reported in the case of Er-doped TiO_2 [9]. This hypothesis is reliable, because of the similarity of the chemical properties of the rare earth elements. In this paper, we used only one path of Sm_2O_3, which was calculated by FEFF. This is a reasonable fitting process, because our only interest currently is relative to Sm-O. Firstly, the Sm_2O_3 powder was fitted as the standard sample. Then, the fabricated samples were fitted by using the parameter of S_0^2 obtained from the fitting of the powder [27]. As shown in Equation (1), S_0^2 is a loss term. There is a parameter in the fitting process termed "*amp* (amplitude)". This *amp* is defined as $amp = S_0^2 \times N_j$. N_j is determined from the standard sample. Fitting the standard sample means obtaining S_0^2, which can be used for fitting other samples because both the standard sample and the fabricated samples are relative to Sm-O. It was hypothesized that there are two patterns of the local structure of Sm: the Sm-O_6 complex with the same distance, and the Sm-O_4 and Sm-O_2 complex bonding Sm with two different distances. Even if the peak was fitted as having the same distance, this does not

mean all of the Sm-O_6 complex actually binds with the same distance, although a benefit of this fitting process is the ease of determining the symmetry.

Table 1 and Table 2 show the bond lengths of the fitting result of A- and R-TiO_2:Sm with different annealing temperatures. The as-deposited sample in Table 1, 400˚C, 900˚C and 1100˚C were fitted using the Sm-O_6 complex with the same distance. As mentioned above, this does not mean all 6 bond lengths were exactly the same distance, but rather enabled easy determination of a change of symmetry state. For relatively highly symmetrical samples, where the distance between the first NN and the second NN is within the fitting error, it is suitable to fit using only one distance. At each temperature, the first NN were 2.41 Å, 2.29 Å, 2.34 Å and 2.41 Å, for as-deposited, 400˚C, 900˚C and 1100˚C samples, respectively, as shown in Table 1. The samples annealed at temperatures of 600˚C, 700˚C and 800˚C were suitable for fitting the Sm-O_6 complex using two distances. For each temperature, the first NN were 2.19 Å, 2.16 Å and 2.37 Å and the second NN were 2.43 Å, 2.63 Å and 2.66 Å, respectively. The distance between the first NN and the second NN were 0.24 Å, 0.47 Å and 0.29 Å. The fitting error of all the fitting results of the first NN was approximately ±0.02 to ±0.04 Å. The fitting error of all results of the second NN was approximately ± 0.05 to ± 0.07 Å. The difference between the distance of the standard value and experimental value should be considered. Even if the standard sample is measured, there is always an error between the standard value and experimental value. The fitting result of the Sm_2O_3 powder, the standard sample, can be used to estimate this error. The standard value of Sm_2O_3 is 2.29 Å and the fitting result

Table 1. The bond length from the fitting result of A-TiO_2:Sm annealed at different temperatures.

Annealing temperature	Fitting result		
	1. The first NN	2. The second NN	Distance between 1 and 2
As-depo	2.41 Å	-	-
400˚C	2.29 Å	-	-
600˚C	2.19 Å	2.43 Å	0.24 Å
700˚C	2.16 Å	2.63 Å	0.47 Å
800˚C	2.37 Å	2.66 Å	0.29 Å
900˚C	2.34 Å	-	-
1100˚C	2.41 Å	-	-

Table 2. The bond length from the fitting result of R-TiO_2:Sm as-deposited and annealed at different temperatures.

Annealing Temperature	Fitting result
	The first NN
As-depo	2.46 Å
400˚C	2.35 Å
600˚C	2.21 Å

was 2.52 Å. Hence, the error was approximately 10 %. The standard value obtained from ATOMS showed that A-TiO_2 consisted of Ti-O_4 of 1.937 Å and Ti-O_2 of 1.966 Å. R-TiO_2 consisted of Ti-O_4 of 1.948 Å and Ti-O_2 1.980 Å. There was also a considerable error of 10% between the standard value and the investigated samples. These differences mainly arose from the XAFS measurements, which exhibited an off-shift from the literature data. There was also a difference in the ionic radii because Sm^{3+} replaced Ti^{4+}. However, these errors do not negate the fitting results. For the A-TiO_2 samples annealed at 600˚C to 800˚C, the distances can be fitted as two lengths, such as Sm-O_4 and longer Sm-O_2, as shown in **Table 1**. This result indicates that the coordination around the Sm atom was more distorted than others, which can be fitted as Sm-O_6 with the same distance. The difference can be estimated within the fitting error or the standard value of the distance between Ti-O_4 and Ti-O_2, and this low symmetrical tendency was increased at an annealing temperature of 700˚C, which was the sample with the most intense PL. This fact reveals the connection between the activation of the Sm luminescent center and the coordination around Sm^{3+} ions. In **Table 2**, the fitting results of the R-TiO_2 are shown and indicate the samples were all highly symmetrical. The analysis of the XANES showed the same result regarding the symmetry, suggesting our prediction was reasonable.

3.4. Discussion

Ishii et al reported the effect of oxidization on the optical and electrical properties. The optimal sample, which was A-TiO_2:Sm annealed at 700˚C for 3 min, is the optimal conditions for exhibiting strong PL emission. On the other word, this sample was sufficiently oxidized to emit intense PL [14].

They also reported that Sm is known to easily form chemical bonds with oxygen and produces large Sm and oxygen complexes, such as SmO_x (generally, $x > 6$). The SmO_x-like complexes are considered to have a definite structure that is determined by the molecules surrounding A-TiO_2, and so a local distortion owing to the complexes produces a uniform trapping level. The optimally oxidized sample has larger A-TiO_2 grains. However, the insufficiently oxidized samples have indefinite coordination numbers, resulting in an optically unfavorable structure. These facts might aid in the energy transfer process of the doped Sm^{3+} ions, giving rise to the intense PL emission.

Figure 7 shows the grain sizes of A- and transition to rutile phase of R-TiO_2:Sm obtained with different annealing temperatures evaluated from XRD patterns [25]. They were estimated according to the Scherrer equation $D = 0.9\lambda/\beta\cos\theta$, where λ is the X-ray wavelength (0.154 nm), β is the FWHM of the XRD, and θ is the diffraction angle. The values of β and θ were taken from A (101) and R (110) diffraction lines. The crystallite diameters of all A-TiO_2:Sm samples annealed at 700˚C to 1000˚C were estimated to be approximately 25.8 nm. There is also a probability that the high crystallinity would result in intense luminescence [24] [32]. For the discussion of this point of view on R-TiO_2, we prepared the

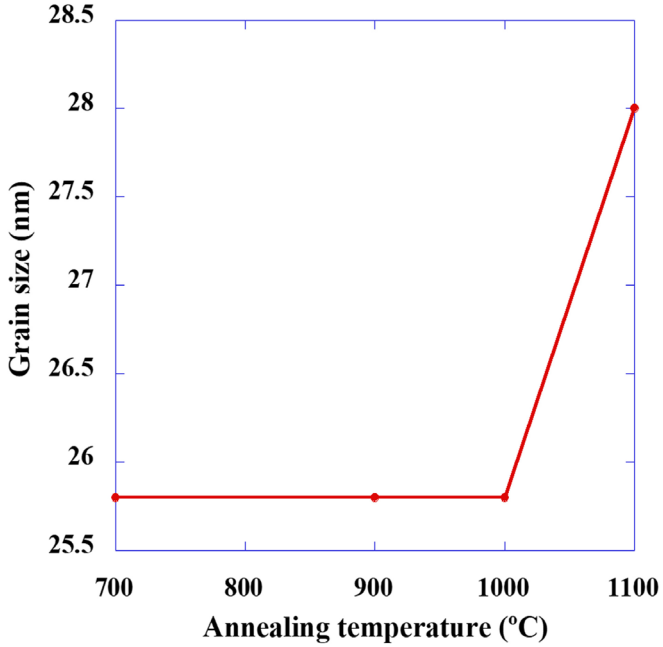

Figure 7. The crystalline diameters of A- and R-TiO_2:Sm obtained with the different annealing temperatures evaluated from XRD patterns according to the Scherrer equation.

A-TiO_2:Sm thin films annealed at 1100˚C, which showed rutile phase of R-TiO_2:Sm in the XRD patterns. This sample can be expected to exhibit higher crystallinity than A-TiO_2:Sm, and the evaluation of its crystallite diameter was 26.3 nm. As a reference, the trapping center of the optically optimal sample is optimally oxidized with larger A-TiO_2 grains, and locally distorted to produce a uniform trapping level [14]. This result and facts indicate the reason that R-TiO_2:Sm shows a weaker PL spectra than A-TiO_2:Sm is not due to the grain sizes being so small that the thin films show weak luminescence, but rather the difference of the crystal symmetry. This indicates that the crystallinity is not the most important factor to achieve an intense PL emission, but rather the atomic coordination around Sm^{3+}.

Hence, the transition probability enables determination of the conditions of materials with an optimal luminous efficiency for application. We have not reached that point in theory, but the symmetry around the doped rare earth element can be shown to be key for obtaining intense luminescence. Further research is required to understand these processes in greater detail.

3.5. Fabrication of a n^+-ITO/TiO_2:Sm/p-NiO/p^+-Si Hetero Junction LED

The result and analysis of PL property and local fine structure revealed the optimal preparing condition, annealing temperature of 700˚C, of A-TiO_2:Sm thin films for enhancing emission. LEDs were prepared under this condition on Si (100) surface. The structure of LED was shown in the inset of **Figure 8**. At first,

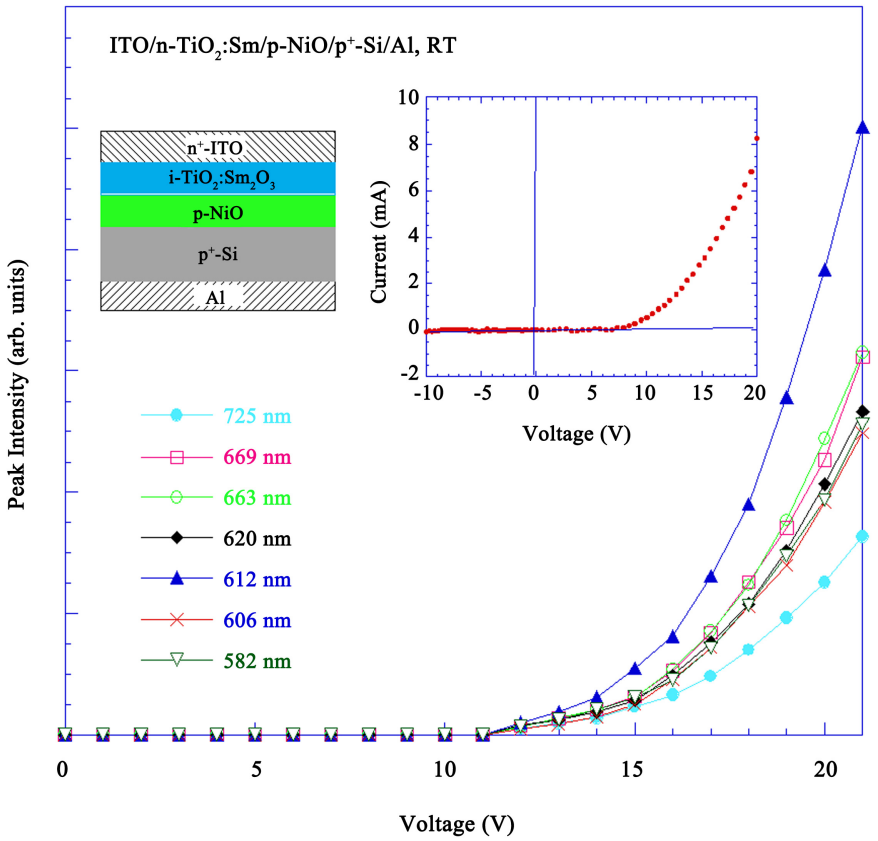

Figure 8. EL intensities of the n^+-ITO/i-TiO_2:Sm/p-NiO/p^+-Si LED at RT at different forward bias voltages. The inset is current-voltage characteristics of the same LED.

140-nm-thick p-NiO thin film was fabricated at the substrate temperature of 150˚C. Then, TiO_2:Sm thin film was formed as the same thickness of p-NiO on NiO surface at RT. Finally, 100-nm-thick transparent ITO layer was formed as a surface electrode. After deposition, the samples were annealed in an O_2 ambient at 700˚C for 3 minutes. Al was selected as a back electrode which was formed 100-nm-thick.

The inset of **Figure 8** shows current-voltage characteristics of the same LED. Threshold was approximately 8 V. This slightly high threshold was due to high electrical resistivity of TiO_2:Sm layer which increased after annealing process. Although, this LED works very well at RT. Also this result suggests that formation of the heterodiode was successfully formed. **Figure 8** shows forward pulse bias dependence of EL intensities of the n^+-ITO/i-TiO_2:Sm/p-NiO/p^+-Si LED measured. Pulsed bias was chosen because of preventing damages to the LED. The EL measurement was started with 12 V at RT. The EL intensity exponentially increased with increasing applied forward voltage. The applied bias voltage dependence was very similar with EL intensity of each peak. This result indicates that a single-typed Sm^{3+} luminescent center was formed. That is the same center which was focused at previous section of PL property and local structure. In addition, EL intensity is corresponding to current injection.

Figure 9 shows EL spectra of the n^+-ITO/i-TiO_2:Sm/p-NiO/p^+-Si LED and PL/CL spectra of a TiO_2:Sm layer such as previous section. A bare TiO_2:Sm sample was excited by using He-Cd laser (325 nm) for measuring PL spectra and by using electron gun (4 KeV), 100 mA/cm^2 for measuring cathodoluminescence (CL) spectra. These three spectra showed similar shapes and their peak positions. It suggests that this EL emission is originated from the same luminescent center of PL and CL. Wider slit was used for detector for EL measurement, hence broadened EL spectra was observed. Moreover, the way of transferring energy to luminescent center of Sm^{3+} was the same. Again, this result indicates that this center is the same one which has been focused at other estimation.

4. Conclusion

Sm^{3+} ions doped anatase (A-) and rutile (R-) TiO_2 thin films were deposited by the laser ablation technique. The crystal phase was selected by controlling the O_2 pressure. After ablation, the samples were annealed at different temperatures, and analyzed by XRD, PL and XAFS. The samples annealed at 700˚C of A-TiO_2 exhibited the strongest PL emission, and the samples annealed at 1100˚C of A-TiO_2 and fabricated as R-TiO_2 crystal phase showed a weak PL emission. The result of the XAFS analysis revealed the local structures of A- and R-TiO_2. The coordination around Sm^{3+} was completely different. The coordination around Sm^{3+} of the samples showing weak PL emission was highly symmetric, and was

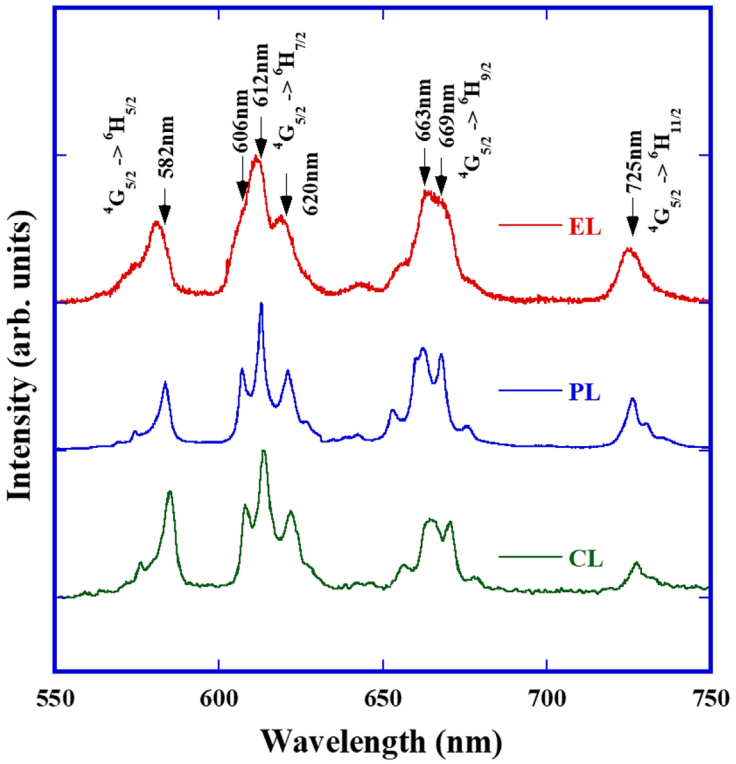

Figure 9. EL, PL, and CL spectra of the n+-ITO/i-TiO_2:Sm/p-NiO/p+-Si LED.

fitted as Sm bonded to six O atoms with the same distance. However, while the Sm^{3+} luminescent center was being activated, the A-TiO_2 samples annealed at 600˚C to 800˚C, and the coordination around Sm^{3+} was distorted. The distances can be fitted as two lengths, Sm-O_4 and longer Sm-O_2. There is the possibility that the higher crystallinity results in more intensive luminescence. A-TiO_2 annealed at 1100˚C, which phase transitioned to the R-TiO_2 sample exhibiting the highest crystallinity, showed that even if the crystallinity was high, the PL emission was not as strong as the A-TiO_2 samples. These facts indicate the strong connection between the activation of the luminescent center and the crystal distortion of the coordination around Sm. The transition possibility has not been determined yet, but fabricating samples with a low symmetry results in the sample having a semi-stable luminescent center which yields an intense PL emission. Based on these results, n^+-ITO/i-TiO_2:Sm/p-NiO/p^+-Si light emitting diode was fabricated with a threshold of approximately 8 V. Clear EL spectra from LED were observed by current injection at RT. Also, single-typed Sm^{3+} luminescent center which was focused at PL property and local structure, was formed. A formation of the heterodiode was successfully formed.

Acknowledgements

The authors would like to thank Mr. Sakurai, Mr. Ohtsuki, and Mr. Aizawa of Tokyo University of Science for the fruitful discussion on previous work. Additionally, we gratefully thank the High Energy Accelerator Research Organization for experimental support and technical advice.

References

[1] Nishikawa, A., Furukawa, N., Kawasaki, T., Terai, Y. and Fujiwara, Y. (2010) Effect of Thermal Annealing on Luminescence Properties of Eu, Mg-Codoped GaN Grown by Organometallic Vapor Phase Epitaxy. *Applied Physics Letters*, **97**, Article ID: 051113. https://doi.org/10.1063/1.3478011

[2] Nyein, E.E., Hömmerich, U., Heikenfeld, J., Lee, D.S., Steckl, A.J. and Zavada, J.M. (2003) Spectral and Time-Resolved Photoluminescence Studies of Eu-Doped GaN. *Applied Physics Letters*, **82**, 1655. https://doi.org/10.1063/1.1560557

[3] Lu, F., Carius, R., Alam, A., Heuken, M. and Buchal, Ch. (2002) Green Electroluminescence from a Tb-Doped AlN Thin-Film Device on Si. *Journal of Applied Physics*, **92**, 2457. https://doi.org/10.1063/1.1497461

[4] Komuro, S., Katsumata, T., Morikawa, T., Zhao, X., Isshiki, H. and Aoyagi, Y. (2000) 1.54 μm Emission Dynamics of Erbium-Doped Zinc-Oxide Thin Films. *Applied Physics Letters*, **76**, 3935. https://doi.org/10.1063/1.126826

[5] Kanjilal, A., Rebohie, L., Skorupa, W. and Helm, M. (2009) Correlation between the Microstructure and Electroluminescence Properties of Er-Doped Metal-Oxide Semiconductor Structures. *Applied Physics Letters*, **94**, 101916. https://doi.org/10.1063/1.3098474

[6] Taguchi, A. and Takahei, K. (1996) Trap Level Characteristics of Rare-Earth Luminescence Centers in III-V Semiconductors. *Journal of Applied Physics*, **79**, 4330. https://doi.org/10.1063/1.361741

[7] Namavar, F., Lu, F., Perry, C.H., Cremins, A., Kalkhoran, N.M. and Soref, R.A. (1995) Strong Room-Temperature Infrared Emission from Er-Implanted Porous Si. *Journal of Applied Physics*, **77**, 4813. https://doi.org/10.1063/1.359403

[8] Minissale, S., Vinh, N.Q., Boer, W., de Bresler, M.S. and Gregorkiewicz, T. (2008) Microscopic Evidence for Role of Oxygen in Luminescence of Er^{3+} Ions in Si: Two-Color and Pump-Probe Spectroscopy. *Physical Review B*, **78**, Article ID: 035313. https://doi.org/10.1103/PhysRevB.78.035313

[9] Ishii, M., Komuro, S. and Morikawa, T. (2003) Study on Atomic Coordination around Er Doped into Anatase- and Rutile- TiO_2:Er-O Clustering Dependent on the Host Crystal Phase. *Journal of Applied Physics*, **94**, 3823. https://doi.org/10.1063/1.1602567

[10] Adler, D.L. Jacobson, D.C., Eaglesham, D.J., Marcus, M.A., Benton, J.L., Poate, J.M. and Citrin, P.H. (1992) Local Structure of 1.54-μm-Luminescence Er^{3+} Implanted in Si. *Applied Physics Letter*, **61**, 2181. https://doi.org/10.1063/1.108288

[11] Frindell, K.L., Bartl, M.H., Robinson, M.R., Bazan, G.C., Popitsch, A. and Stucky, G.D. (2003) Visible and Near-IR Luminescence via Energy Transfer in Rare Earth Doped Mesoporous Titania Thin Films with Nanocrystalline Walls. *Journal of Solid State Chemistry*, **172**, 81-88. https://doi.org/10.1016/S0022-4596(02)00126-3

[12] Ting, C.C., Chen, S.Y. and Lee, H.Y. (2003) Physical Characteristics and Infrared Fluorescence Properties of Sol-Gel Derived Er^{3+}-Yb^{3+} Codoped TiO_2. *Journal of Applied Physics*, **94**, 2102. https://doi.org/10.1063/1.1590411

[13] Stouwdam, J.W. and van Veggel, F.C.J.M. (2004) Sensitized Emission in Ln^{3+}-Doped TiO_2 Semiconductor Nanoparticle. *ChemPhysChem*, **5**, 743-746. https://doi.org/10.1002/cphc.200300967

[14] Ishii, M., Towlson, B., Poolton, N., Harako, S., Zhao, X., Komuro, S. and Hamilton, B. (2012) Effects of Oxidization and Deoxidization on Charge-Propagation Dynamics in Rare-Earth-Doped Titanium Dioxide with Room-Temperature Luminescence. *Journal of Applied Physics*, **111**, Article ID: 053514. https://doi.org/10.1063/1.3691241

[15] Michel, J., Benton, J.L., Ferrante, R.F., Jacobson, D.C., Eaglesham, D.J., Fitzgerald, E.A., Xie, Poante, Y.-H.J.M. and Kimerling, L.C. (1991) Impurity Enhancement of the 1.54-μm Er^{3+} Luminescence in Silicon. *Journal of Applied Physics*, **70**, 2672. https://doi.org/10.1063/1.349382

[16] Chen, S.Y., Ting, C.C. and Li, C.H. (2002) Fluorescence Enhancement and Structural Development of Sol-Gel Derived Er^{3+}-Doped SiO_2 by Yttrium Codoping. *Journal of Materials Chemistry*, **12**, 1118-1123. https://doi.org/10.1039/b107380j

[17] Shi, E., Zhang, L., Li, Z., Li, P., Shang, Y., Jia, Y., Wei, J., Wang, K., Zhu, H., Wu, D., Zhang, S. and Cao, A. (2012) TiO_2-Coated Carbon Nanotube-Silicon Solar Cells with Efficiency of 15%. *Scientific Reports*, **2**, Article No. 884. https://doi.org/10.1038/srep00884

[18] Holland, L., Laurenson, L., Baker, P.N. and Davis, H.J. (1972) Electrochemical Photolysis at Water at a Semiconductor Electrode. *Nature*, **238**, 37-38.

[19] Fujishima, A., Zhang, X. and Tryk, D.A. (2008) TiO_2 Photocatalysis and Related Surface Phenomena. *Surface Science Reports*, **63**, 515-582. https://doi.org/10.1016/j.surfrep.2008.10.001

[20] Ohsaka, T., Izumi, F. and Fujiki, Y. (1978) Raman Spectrum of Anatase, TiO. *Journal of Raman Spectroscopy*, **7**, 321-324.

[21] Rosa-Cruz, E., De la Torres, L.A., Diaz Salas, P., Rodŕıguez, R.A., Kumar, G.A.,

Meneses, M.A., Mosi-o, J.F., Hernández, J.M. and Barbosa-Garćıa, O. (2003) Luminescent Properties and Energy Transfer in ZrO_2:Sm^{3+} Nanocrystals. *Journal of Applied Physics*, **94**, 3509-3515. https://doi.org/10.1063/1.1599960

[22] Kiisk, V., Sildos, I., Reedo, V., Tätte, T., Kirm, M. and Aarik (2005) Photoluminescence Characterization of Pure and Sm^{3+}-Doped Thin Metaloxide Films. *Applied Surface Science*, **247**, 412-417. https://doi.org/10.1016/j.apsusc.2005.01.076

[23] Lin, H., Yang, D., Liu, G., Ma, T., Zhai, B., An, Q., Yu, J., Wang, X., Liu, X. and Pun, E.B.-Y. (2005) Optical Absorption and Photoluminescence in Sm^{3+}- and Eu^{3+}-Doped Rare-Earth Borate Glasses. *Journal of Luminescence*, **113**, 121-128. https://doi.org/10.1016/j.jlumin.2004.09.115

[24] Jing, F., Harako, S., Komuro, S. and Zhao, X. (2009) Luminescence Properties of Sm^{3+}-Doped TiO_2 Thin Films Prepared by Laser Ablation. *Journal of Physics D*, **42**, Article ID: 085109. https://doi.org/10.1088/0022-3727/42/8/085109

[25] Sakurai, J., Harako, S., Ohtsuki, T., Komuro, S., Hirao, N., Kasahara, R. and Zhao, X. (2012) Photoluminescence and X-Ray Absorption Fine Structure Analysis of Sm-Doped TiO_2 Thin Films. *Japanese Journal of Applied Physics*, **51**, 06FG03. https://doi.org/10.1143/JJAP.51.06FG03

[26] Ishii, M., Crowe, I.F., Halsall, M.P., Hamilton, B., Hu, Y., Sham, T.-K., Harako, S., Zhao, X. and Komuro, S. (2013) Atomic-Scale Distortion of Optically Activated Sm Dopants Identified with Site-Selective X-Ray Absorption Spectroscopy. *Journal of Applied Physics*, **114**, Article ID: 133505. https://doi.org/10.1063/1.4824375

[27] Piamonteze, C.A., Iniguez, C., Tessler, R.L., Alves, M.C.M. and Tolentino, H. (1998) Environment of Erbium in a-Si:H and a-SiOx:H. *Physical Review Letters*, **81**, 4652-4655.

[28] Ankudinov, A.L., Ravel, B., Rehr, J.J. and Conradson, S.D. (1998) Real-Space Multiple-Scattering Calculation and Interpretation of X-Ray-Absorption Near-Edge Structure. *Physical Review B*, **58**, 7565-7576. https://doi.org/10.1103/PhysRevB.58.7565

[29] Ankudinov, A.L., Bouldin, C.E., Rehr, J.J., Sims, J. and Hung, H. (2002) Parallel Calculation of Electron Multiple Scattering Using Lanczos Algorithms. *Physical Review B*, **65**, Article ID: 104107. https://doi.org/10.1103/PhysRevB.65.104107

[30] Binsted, N., Strange, R.W. and Hasnain, S.S. (1992) Constrained and Restrained Refinement in EXAFS Data Analysis with Curved Wave Theory. *Biochemistry*, **31**, 12117-12125. https://doi.org/10.1021/bi00163a021

[31] Aizawa, Y., Ohtsuki, T., Harako, S., Komuro, S., Hirao, N. and Zhao, X. (2014) Sensitization Effect of Al Co-Doping on Nd-Related Photoluminescence in TiO_2 Matrix. *Japanese Journal of Applied Physics*, **53**, 06JG06. https://doi.org/10.7567/JJAP.53.06JG06

[32] Kuo, S.Y. and Hsieh, W.F. (200) Structural and Optical Properties of Erbium-Doped $Ba_{0.7}Sr_{0.3}TiO_3$ Thin Films. *Journal of Vacuum Science & Technology A*, **23**, 768-772.